Generation of Noninductive Current by Electron-Bernstein Waves on the COMPASS-D Tokamak

V. Shevchenko,[1] Y. Baranov,[1] M. O'Brien,[1] and A. Saveliev[2]

[1]*EURATOM/UKAEA Fusion Association, Culham Science Centre, Abingdon, OX14 3DB, United Kingdom*

[2]*Ioffe Institute, Politekhnicheskaya 26, 194021 St. Petersburg, Russia*

(Received 24 July 2002; revised manuscript received 7 October 2002; published 10 December 2002)

Electron-Bernstein waves (EBW) were excited in the plasma by mode converted extraordinary (X) waves launched from the high field side of the COMPASS-D tokamak at different toroidal angles. It has been found experimentally that X-mode injection perpendicular to the magnetic field provides maximum heating efficiency. Noninductive currents of up to 100 kA were found to be driven by the EBW mode with countercurrent drive. These results are consistent with ray tracing and quasilinear Fokker-Planck simulations.

DOI: 10.1103/PhysRevLett.89.265005 PACS numbers: 52.35.Hr, 52.50.Sw, 52.65.Ff

Electron-Bernstein waves (EBW) experience very localized damping on electrons at the electron cyclotron resonance but, unlike the extraordinary (X) mode and the ordinary (O) mode, the damping remains strong even at high harmonics of the electron cyclotron (EC) frequency ω_{ce}. EBW do not have any density cutoffs inside the plasma and can, therefore, access plasmas of arbitrary densities for frequencies above ω_{ce}. These features of EBW present the possibility of efficient means for electron cyclotron resonance heating (ECRH) and current drive in high beta plasmas, particularly in spherical tokamaks, where the X-mode and O-mode propagation into the plasma can be assured only at high ω_{ce} harmonics leading to weak damping of these modes inside the plasma. Plasma heating with the use of EBW excitation via the O-X-B mode conversion mechanism has been successfully demonstrated on the W7-AS stellarator [1]. EBW heating experiments with direct mode conversion of the X mode, launched from the high field side (HFS), to the EBW mode were carried out on the WT-3 tokamak [2]. In the present Letter, we present the first results of EBW heating and current drive experiments conducted on the COMPASS-D tokamak. COMPASS-D [3] presents a possibility for EBW excitation via direct mode conversion of the X mode, launched from the HFS, to the EBW mode at the upper hybrid resonance (UHR), allowing us to study EBW plasma heating and current drive (see Fig. 1). According to cold plasma theory, the X mode is subject to very weak damping at the ω_{ce} resonance for launch angles nearly perpendicular to the magnetic field. Hence, the X mode propagates to the UHR where it is always totally converted to the EBW mode, with further absorption near the ω_{ce} resonance. At launch angles far from perpendicular, the X-mode absorption becomes stronger, resulting in predominant X-mode plasma heating. By varying the toroidal launch angle, one can estimate the relative heating and current drive efficiencies of the X mode and the EBW mode.

A highly reproducible plasma scenario has been chosen for target plasma generation during these experiments (see Fig. 2). The line averaged density, plasma current, and central toroidal field were sustained at 1.8×10^{19} m^{-3}, 150 kA, and 2.05 T, respectively. A power of 600 kW at a frequency $\omega/2\pi$ of 60 GHz with a constant pulse duration of 100 ms was injected into the plasma at the beginning of the flattop (100 ms) of plasma current and density. The toroidal launch angle was changed shot by shot in the range $\pm 32.6°$ from perpendicular, with a step of $\sim 8.4°$. ECRH power was injected with polarization perpendicular to the magnetic field. Electron temperature T_e and density profiles n_e were measured with multipoint Thomson scattering (TS) every 50 ms. During ECRH, the electron temperature appears to be noticeably

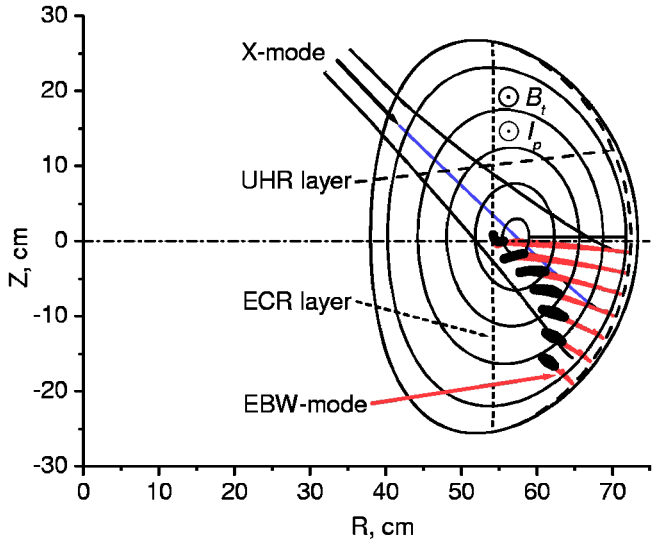

FIG. 1 (color online). Poloidal projection of EBW ray-tracing results for the X mode launched from the HFS perpendicularly to the magnetic field. Black areas correspond to strong damping of EBWs.

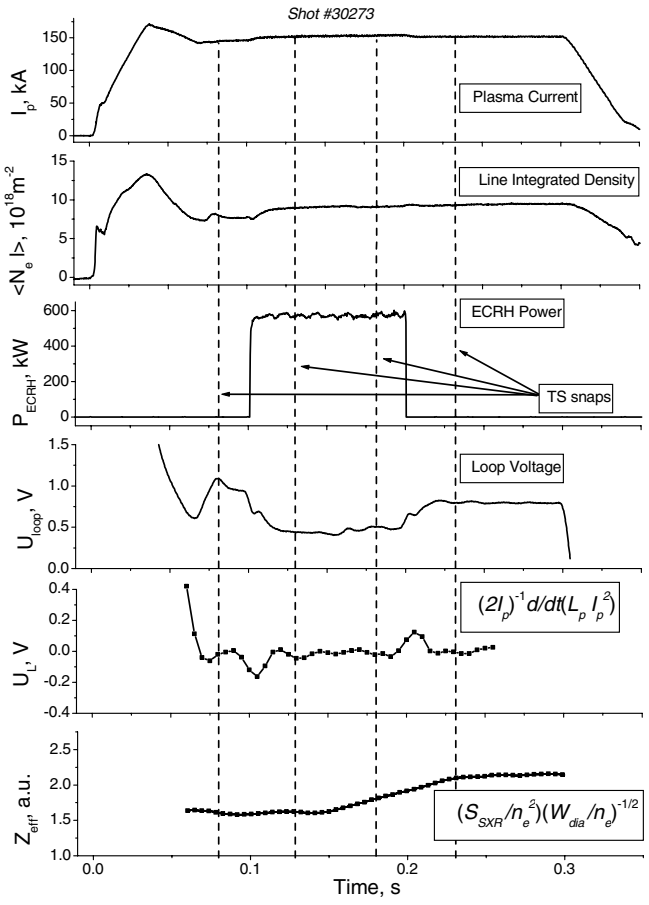

FIG. 2. Waveforms of main plasma parameters during EBW experiments on COMPASS-D.

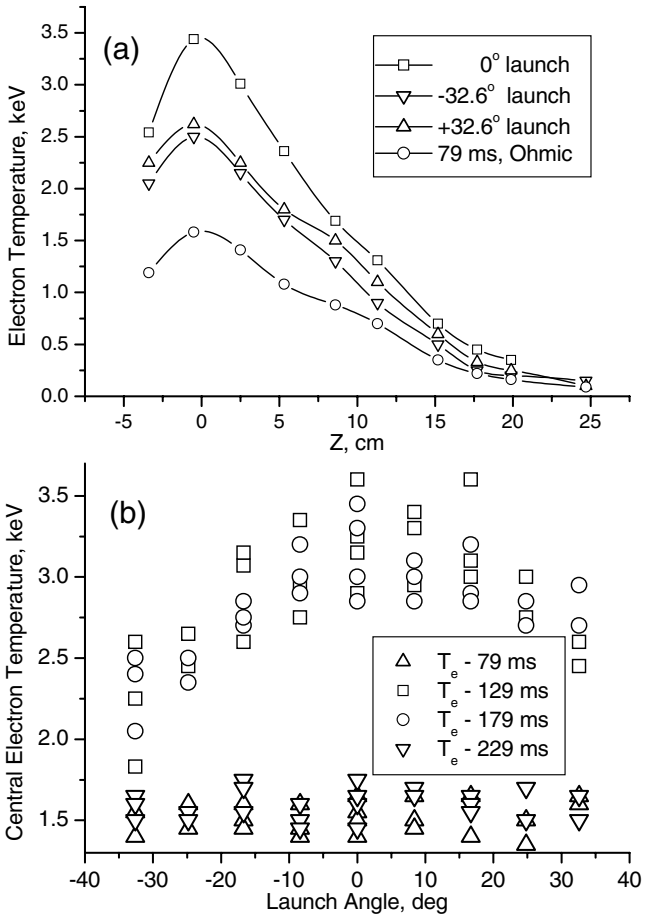

FIG. 3. (a) Electron temperature profiles measured with and without ECRH. (b) Central electron temperature at different times versus toroidal launch angle (measured from perpendicular). Vertical size of the symbols corresponds to the typical error bars of TS measurements.

higher for launch angles close to perpendicular to the magnetic field, while the electron temperature profiles do not show any significant transformation, such as peaking or flattening, over the whole range of launch angles [see Fig. 3(a)]. The central electron temperature, measured during ECRH, is plotted as a function of launch angle in Fig. 3(b). The clear maximum at 0° launch angle indicates higher heating efficiency with EBW excitation than with the X-mode heating alone. The excess of the maximum in electron temperature at perpendicular launch is well above the error bars of the TS measurements. The temperature was measured at 2 times during the ECRH pulse. The electron temperature measured at 129 ms has the same dependence on the launch angle as the temperature measured at 179 ms, so, evidently, enhanced plasma heating with perpendicular injection is not a transient effect.

Changes in the surface loop voltage, V_{loop}, required to maintain constant plasma current during ECRH, do not have any obvious dependence on the launch angle. Typically the plasma was sustained at a central electron temperature of 1.5 keV and a loop voltage of about 0.9 V before ECRH injection. During ECRH the loop voltage usually dropped down to the value of 0.5 V with slight variations within 0.1 V over the range of launch angles. Because of the temperature changes, one would expect much greater reductions in the loop voltage, especially at launch angles close to perpendicular when the electron temperature reaches 3.5 keV. For instance, the loop voltage drops down to values less than 250 mV when ECRH of the same power is employed at $2\omega_{ce}$ in plasmas with similar current and electron temperature before and during ECRH injection. Such a big drop in loop voltage is consistent with the plasma resistance ($\sim T_e^{-3/2}$) reduction during second harmonic ECRH .

Using the Poynting formulation for the plasma power balance, we have

$$V_{\text{loop}} = V_{\text{res}} + \frac{1}{I_p}\frac{d}{dt}\left(\frac{LI_p^2}{2}\right), \tag{1}$$

where the first term V_{res} is the voltage drop due to the plasma resistance and the second term is responsible for the voltage drop due to plasma current I_p and plasma inductance L variations. The plasma inductance is obtained from the magnetic equilibrium reconstruction. Typical behavior of the inductive term during ECRH is shown in Fig. 2. One can see that loop voltage variations

due to the inductive part are significant only transiently when ECRH is switched on and off, while in the middle of the ECRH pulse the induced voltage is close to zero. Thus, we can conclude that the loop voltage variations during ECRH are mainly defined by the plasma conductivity changes and noninductive currents driven in the plasma. The plasma conductance ($\sigma_p \sim Z_{\rm eff}^{-1} T_e^{3/2}$) variations can be attributed only to the effective plasma ion charge $Z_{\rm eff}$ and T_e. $Z_{\rm eff}$ behavior during the shot can be analyzed qualitatively with the use of soft x-ray ($S_{\rm SXR}$) signals. T_e and n_e profile shapes are measured not to change during the ECRH pulse, and we assume that the $Z_{\rm eff}$ profile also remains unchanged. Using relations for measured $S_{\rm SXR}$ and plasma diamagnetic energy $W_{\rm dia}$: $S_{\rm SXR} \sim Z_{\rm eff} n_e^2 T_e^{1/2}$ and $W_{\rm dia} \sim n_e T_e$, one can write $Z_{\rm eff} \sim (S_{\rm SXR}/n_e^2)(W_{\rm dia}/n_e)^{-1/2}$. Estimations, conducted in this way, indicate an almost constant value of $Z_{\rm eff}$ during the first half of the ECRH pulse and a gradual increase during the second half with some remaining growth afterwards, as illustrated in Fig. 2. $Z_{\rm eff}$ reaches a new stationary value typically ~30 ms after the ECRH pulse. The total growth is usually about 25%, which can be attributed to the increase of the impurity flux from the antenna during ECRH injection and afterwards. Thus, assuming for simplicity that $Z_{\rm eff}$ does not change during the shot, the noninductive current driven in the plasma can be estimated from the experimental $V_{\rm loop}$ and T_{e0} with the use of the simple relation,

$$I_{\rm CD} = I_p - I_{\rm BS}^{\rm ECRH} - (I_p - I_{\rm BS}^{\rm OH}) \frac{V_{\rm loop}^{\rm ECRH}}{V_{\rm loop}^{\rm OH}} \left(\frac{T_{e0}^{\rm ECRH}}{T_{e0}^{\rm OH}} \right)^{3/2}, \quad (2)$$

where the plasma current I_p is fixed (150 kA), and the bootstrap current $I_{\rm BS}^{\rm OH}$ during the Ohmic heating phase, as estimated with the Fokker-Plank code [4], is about 12 kA, while during ECRH it varies from 15 to 21 kA over the range of launch angles. In order to take into account the small $Z_{\rm eff}$ growth during the second half of the ECRH pulse and afterwards, the correction factor $Z_{\rm eff}^{\rm OH}/Z_{\rm eff}^{\rm ECRH}$ has to be applied to the last term in formula (2). The results are plotted in Fig. 4, from which it is clear that quite a large current, up to 100 kA, must be driven in a direction counter to the plasma current in order to maintain almost constant loop voltage over the range of electron temperatures during ECRH. The maximum of the driven current corresponds to launch angles close to perpendicular to the magnetic field. At perpendicular launch, only a small fraction of the injected power ($\lesssim 10\%$) is absorbed in the plasma as the X mode, while the main part of the power is converted into the EBW mode and then absorbed near the $\omega_{\rm ce}$ resonance. This indicates that the EBW mode is responsible for the noninductive current driven in this case. The scatter in the driven current estimated from experimental data can mainly be attributed to the scatter in electron temperature measurements. TS measurements are taken instantly and the result is very sensitive to the plasma activity. The other experimental measurements used in the above analysis are typically averaged over the plasma volume or smoothed in time.

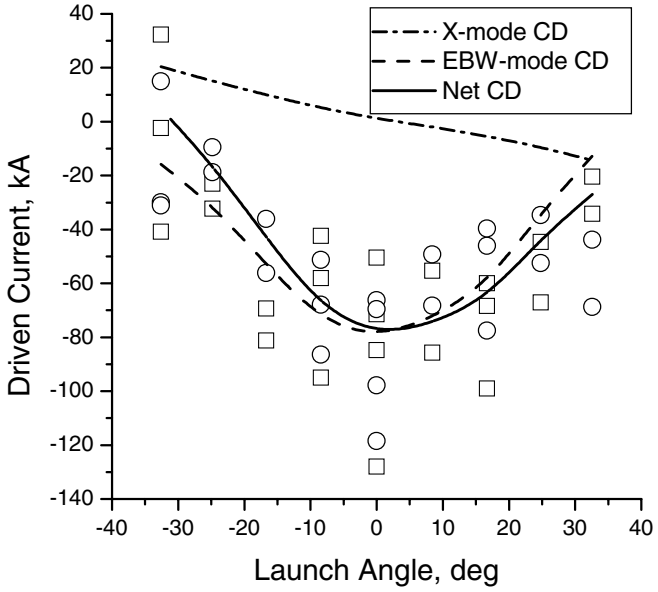

FIG. 4. Noninductive current driven in the plasma estimated from experimental data and ray-tracing results for currents driven by the X mode, the EBW mode alone, and the net current due to ECRH. Circles and squares correspond to time slices as in Fig. 3.

A new EBW ray-tracing code has been developed for EBW current drive (CD) modeling in COMPASS-D. The plasma equilibrium obtained from magnetic equilibrium reconstruction and the electron density and temperature profiles measured with TS were used as input parameters for the EBW ray-tracing code. This code allows estimation of power deposition profiles with relevant wave vector k profiles for both the X mode and the EBW mode in a full tokamak equilibrium. These results have been used as input data for a quasilinear relativistic Fokker-Planck code [5], modified for EBW applications, in order to simulate currents driven by the X mode and by the EBW mode alone. The results of EBW CD modeling including trapped electron effects are summarized in Fig. 4. The X-mode driven current spans the range from -14 to $+20$ kA and becomes zero at angles close to perpendicular to the magnetic field. The current driven by EBW does not change sign over the range of launch angles and reaches a maximum of about -80 kA at perpendicular launch. The net ECRH driven current is predominantly defined by the EBW fraction and is in good agreement with experimental results. Estimates of the normalized experimental EBW current drive efficiency give the value of $\eta_{20\rm CD} = R_0 n_e I_{\rm CD}/P_{\rm ECRH} \approx 0.035$ (10^{20} A/W m^2), which is higher than the typical figure for O/X-mode current drive but less efficient than for lower hybrid current drive.

It was found from modeling that with the existing antenna setup the EBW power deposition profile is located well below the midplane for all negative and positive

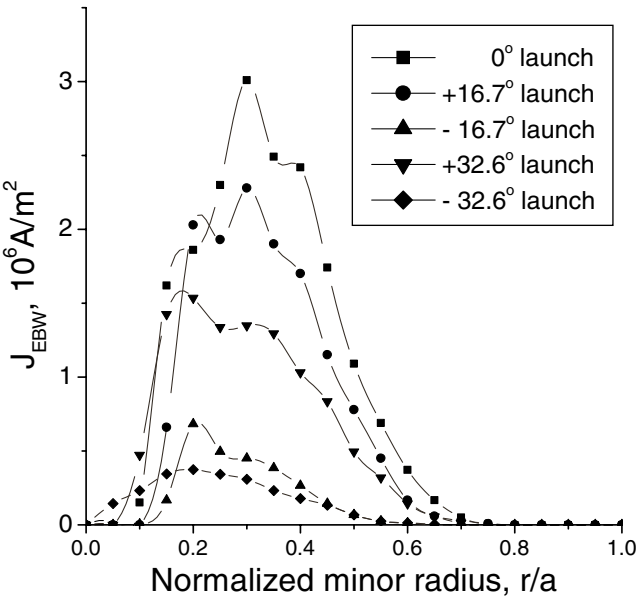

FIG. 5. The radial profiles of the current density generated by EBW mode alone for different launch angles.

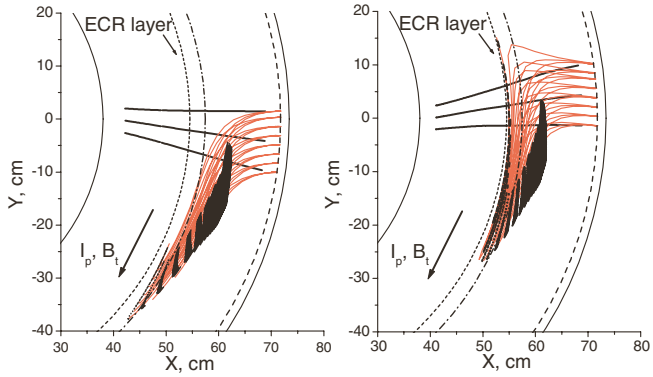

FIG. 6 (color online). Toroidal projections of EBW ray-tracing results for toroidal launch angles of −16.7° (left) and +16.7° (right). Black areas correspond to strong damping of EBWs, where $k_\| > 0$ and $\omega > \omega_{ce}$. Note $\mathrm{sgn}(I_{CD}) = \mathrm{sgn}[k_\|/(\omega_{ce} - \omega)]$.

toroidal launch angles (see Fig. 1). EBW driven current is distributed in the range of $0.05a$ to $0.7a$ with the maximum at the radius of $0.3a$ as illustrated in Fig. 5. Interestingly, for the HFS launch geometry in COMPASS-D the $k_\| = (k \cdot B)/|B|$ (here B is a vector of local magnetic field) related to the EBW fraction always becomes positive as the wave approaches the EC resonance independent of the toroidal launch angle, and it changes sign to negative if the plasma current is reversed. In other words, for the existing launch configuration, Bernstein waves always drive current in the direction counter to the plasma current (see Fig. 6). This is because of the influence of the poloidal field as described below. The predicted magnitude of the current driven by EBW is proportional to the power of the X mode reaching the UHR layer. The sign of the driven current depends only on the EBW power deposition profile with respect to the midplane or more precisely to the magnetic axis. The power absorbed in the plasma above the midplane generates current in the codirection, while the power absorbed below the midplane always generates current in the counterdirection. A similar result has been numerically obtained for EBW launched off midplane perpendicularly to the magnetic field [6]. Our modeling shows that the direction of EBW CD changes to opposite if the direction of the toroidal field is reversed. Unfortunately, experiments with reversed toroidal magnetic field have not been possible. In general, the sign of the driven current is determined by the sign of $k_\|/(\omega_{ce} - \omega)$ in the absorption region. In tokamak plasmas usually $B_\varphi \gg B_\theta$, where φ and θ are the toroidal and poloidal components, respectively, hence, $k_\| \approx k_\varphi + k_\theta B_\theta/|B|$. In the UHR layer EBW has typically $|k_\theta B_\theta/|B|| \gg |k_\varphi|$, except for the vicinity of the midplane, thus the sign of $k_\|$ is mainly determined by the sign of $k_\theta B_\theta/|B|$. As EBW propagates deeper into the plasma, k_θ is developed, due to poloidal plasma inhomogeneity, resulting in a different sign of $k_\|$ above and below the midplane. Moreover, $k_\theta B_\theta/|B|$ changes sign if the plasma current is reversed and remains unchanged if the toroidal field is reversed.

In summary, we have shown that the perpendicularly launched X mode from the HFS of the tokamak provides more efficient plasma heating at fundamental EC resonance in comparison with the angular launch. Noninductive currents up to 100 kA were found to be driven in the direction counter to the Ohmic current. Mainly EBWs, which are efficiently mode converted from the X mode in the UHR layer, are responsible for CD induced in the plasma. The results are in good agreement with EBW ray tracing and nonlinear Fokker-Plank modeling.

The authors thank Professor A. D. Piliya for his crucial role in the EBW ray-tracing code development, and Dr. M. Shoucri and Dr. I. Shkarovsky for providing the Fokker-Planck code. This work was jointly funded by U.K. Department of Trade Industry and EURATOM.

[1] H. P. Laqua *et al.*, Phys. Rev. Lett. **78**, 3467 (1997).
[2] T. Maekawa *et al.*, Phys. Rev. Lett. **86**, 3783 (2001).
[3] G. A. Whitehurst *et al.*, in *Proceedings of the 22nd EPS Conference on Controlled Fusion and Plasma Physics, Bournemouth, 1995* (The European Physical Society, Abingdon, United Kingdom, 1995), Vol. 19C, p. I-345.
[4] M. O'Brien *et al.*, in *Proceedings of IAEA TCM on Advanced Simulations and Modelling of Thermonuclear Plasma, Montreal, 1992* (IAEA, Vienna, 1993), p. 527.
[5] M. Shoucri and I. Shkarovsky, Comput. Phys. Commun. **82**, 287 (1994).
[6] C. B. Forest *et al.*, Phys. Plasmas **7**, 1352 (2000).